Amino Acids (2013) 44:1233–1240
DOI 10.1007/s00726-012-1445-1

SHORT COMMUNICATION

Phosphorylation of nuclear and cytoplasmic pools of ribosomal protein S6 during cell cycle progression

Margit Rosner · Katharina Schipany · Markus Hengstschläger

Received: 28 September 2012 / Accepted: 7 December 2012 / Published online: 20 December 2012

Abstract Of all known ribosomal proteins, the 40S ribosomal protein S6 is by far the most extensively studied. Still, little is known about some basic aspects of S6 regulation including its cell cycle-related expression and localization. Using a flow cytometric single cell approach applied to whole cells and isolated nuclei, we monitored nucleocytoplasmic expression of total and S240/4 phosphorylated S6 during unperturbed cell cycle progression, providing first evidence for a S6-specific spatiotemporal pattern and its deregulation under conditions of hyperactivated mTOR.

Keywords S6 serine 240/4 · mTOR · TSC1/2 · Cell cycle · Nucleocytoplasmic · Phospho-flow

Introduction

Ribosome biogenesis is a dynamic multistep process and involves the coordinated interplay between ribosomal RNA, ribosomal proteins (RPs), and numerous co-factors. Among eukaryotic RPs, it is the 40S ribosomal protein S6 (S6), which, for several reasons, has attracted most attention: (1) S6 was the first RP demonstrated to undergo inducible phosphorylation upon various stimuli, including growth factors, cytokines, hormones, nutrients, and lipid compounds; (2) unlike other RPs, S6 is indispensable since heterozygosity was shown to cause early embryonic lethality in mice (Meyuhas 2008); (3) it is the best-known substrate of the ribosomal protein S6 kinases (S6Ks), which are direct effectors of the mechanistic target of rapamycin complex 1 (mTORC1). Upon integration of several signaling cascades, mTORC1 senses mitogen, nutrient, and energy availability to control fundamental cellular processes such as protein synthesis, cell growth, cell cycle progression, and overall cell metabolism (Ma and Blenis 2009; Laplante and Sabatini 2012); (4) although phosphorylation of mTOR at several sites has been described, none of these reliably correlates with mTORC1-specific kinase activity, making the technically feasible investigation of phosphorylated S6, a valuable readout for mTORC1 activity. Since hyperactivation of the mTOR pathway is a hallmark of many cancers and genetic diseases, S6 is widely used as diagnostic and therapeutic biomarker to prove mTOR deregulation in tumor specimens or to monitor drug responses (Meyuhas 2008; Ma and Blenis 2009; Perl et al. 2012).

Ras/Raf/MEK/ERK and PI3K/AKT/TSC2/mTOR pathways converge on the level of S6 to promote its phosphorylation at S235/6 and S240/4. Whereas S6K targets both sites, p90 ribosomal S6 kinase (RSK), the substrate of extracellular signal-regulated kinase (ERK), was shown to exclusively phosphorylate S235/6, rendering S240/4 the more specific readout for mTORC1-dependent S6K activity (Roux et al. 2007; Ma and Blenis 2009). Whereas S6 phosphorylation and its regulatory inputs have been extensively studied, its physiological roles are not yet entirely understood (Meyuhas 2008).

In contrast, S6 nucleocytoplasmic shuttling in the context of ribosome biogenesis is well defined. Following translation in the cytoplasm and involving specific nuclear and nucleolar localization sequences, S6 is actively targeted to the nucleolus where it assembles into 40S preribosomal subunits. Nascent subunits are translocated to the nucleoplasm, what induces a specific ribosomal maturation

M. Rosner · K. Schipany · M. Hengstschläger (✉)
Institute of Medical Genetics, Medical University of Vienna, Währinger Strasse 10, 1090 Vienna, Austria
e-mail: markus.hengstschlaeger@meduniwien.ac.at

pathway. Ripening preribosomal subunits shuttle back to the cytoplasm and finally fuse with 60S ribosomal subunits to form mature, functional ribosomes (Krüger et al. 2007; Kundu-Michalik et al. 2008; Cisterna and Biggiogera 2010).

Loss of S6 is known to cause impaired 40S ribosome biogenesis and the induction of nucleolar stress, which triggers a specific pathway involving ribosomal protein L11, MDM2, and p53 to induce G1 cell cycle arrest (Fumagalli et al. 2009; Zhang and Lu 2009). Although the cell cycle-regulating properties of S6 are well documented, little is known about its regulation during cell cycle progression. Using traditional serum starvation approaches, it was demonstrated that S6 phosphorylation is strongly induced upon serum-mediated re-entry of quiescent fibroblasts into the cell cycle (Martin-Pérez and Thomas 1983; Rosner and Hengstschläger 2010). Although this approach is well proven for the identification of G0/G1-regulated events, one of its limitations concerns the rapid decline of cell synchrony at the G1/S transition, which makes proper evaluation of S and G2/M phases difficult.

Flow cytometry employing phosphosite-specific antibodies (phospho-flow) is an increasingly accepted method for evaluation of signaling events and therapeutic drug monitoring at the single cell level (Perl et al. 2012; Bendall and Nolan 2012). In this study, we made use of a specific combination of flow cytometric protein, DNA, and cell size (FSC; forward scatter) analyses to establish an expression map of total and phosphorylated S6 during normal cell cycle progression at high resolution. Analyzing asynchronous cells of different origin, we here identify S6 phosphorylation at S240/4 as being strongly cell cycle-regulated and provide evidence for its deregulation under conditions of mTOR hyperactivation. Simultaneous evaluation of whole cells and isolated nuclei allowed to additionally draw conclusions on the corresponding nucleocytoplasmic distribution and finally revealed a specific, spatiotemporal pattern of total and phosphorylated S6. Unlike traditional methods, our approach is devoid of any synchronization procedures and yields information on the cell cycle regulation of nucleocytoplasmic S6 in actively dividing, unperturbed cells. Thus, our data more closely resemble the in vivo situation, what might be of overall relevance for the in-depth understanding of both, S6 regulation and function.

Materials and methods

Cell culture

Immortalized p53-positive *TSC1* (hamartin) and p53-negative *TSC2* (tuberin) wildtype and knockout mouse embryonic fibroblasts (MEFs) were grown in Dulbecco's modified eagle medium (DMEM) (PAA), supplemented with 10 % FCS. The monoclonal human amniotic fluid stem (hAFS) cell line Q1 was maintained in α-MEM minimal essential medium (Life Technologies), supplemented with 15 % fetal bovine serum (HyClone), 18 % Chang B, and 2 % Chang C (Irvine Scientific). Human BxPC-3 pancreatic adenocarcinoma cells (ATCC CRL-1687) were grown in RPMI (PAA), supplemented with 10 % FCS. All media were additionally supplemented with 2 mM glutamine, 50 mg/l streptomycin sulfate and 30 mg/l penicillin. Cells were kept in a humidified incubator with 5 % atmospheric CO_2.

Antibodies

Primary antibodies used in (or applicable for) both, flow cytometry and immunoblotting approaches, include α-tubulin (clone DM1A) (#CP06, Calbiochem), fibrillarin (clone C13C3) (#2639, Cell Signaling), S6 ribosomal protein (clone 54D2) (#2317, Cell Signaling), and S6 ribosomal protein S240/244 (clone D68F8) (#5364, Cell Signaling). Species- and subtype-matched control immunoglobulins, including a rabbit monoclonal isotype control (clone DA1E) (#3900, Cell Signaling) and a mouse monoclonal IgG_1 isotype control (clone G3A1) (#5415, Cell Signaling), were used as negative controls in flow cytometry. The following secondary antibody reagents for flow cytometric and immunoblot analyses, comprising Alexa Fluor 488 and HRP conjugates, were used: goat anti-rabbit IgG (H+L), $F(ab')_2$ fragments, Alexa Fluor 488 conjugate (#4412, Cell Signaling), goat anti-mouse IgG (H+L), $F(ab')_2$ fragments, Alexa Fluor 488 conjugate (#4408, Cell Signaling), goat anti-rabbit IgG (H+L), HRP conjugate (#A120-101P, Bethyl Laboratories) and goat anti-mouse IgG (H+L), HRP conjugate (#A90-116P, Bethyl Laboratories).

Preparation of whole cell lysates and immunoblotting

Whole cell lysates containing both, cytoplasmic and nuclear proteins, were prepared by physical disruption of cell membranes by repeated freeze and thaw cycles. Briefly, cells were washed with cold PBS and harvested by rapid and gentle trypsinization at room temperature. Pellets were washed twice with ice-cold PBS and lysed in whole cell extraction buffer containing 20 mM Hepes, pH 7.9, 0.4 M NaCl, 25 % glycerol, 1 mM EDTA, 0.5 mM dithiothreitol, 1 mM phenylmethylsulfonyl fluoride, 0.5 mM NaF, 0.5 mM Na_3VO_4 supplemented with 2 μg/ml aprotinin, 2 μg/ml leupeptin, 0.3 μg/ml benzamidinchlorid, 10 μg/ml trypsininhibitor by freezing and thawing. Supernatants were collected by centrifugation at 20,000*g* for 20 min at 4 °C. Denatured samples were resolved by

standard SDS-polyacrylamide gel electrophoresis and transferred to nitrocellulose membranes. Membranes were incubated with antibodies described in the Antibodies section and immunodetection was performed via autoradiography using the enhanced chemiluminescence method (Pierce) already earlier described (Rosner and Hengstschläger 2011).

Isolation of intact cell nuclei via biochemical fractionation

Adherent cells were washed with cold PBS and harvested by rapid and gentle trypsinization at room temperature. Detaching cells were resuspended in cold, serum-containing growth medium, pelleted by centrifugation (200*g*; 2 min; 4 °C) and washed once with cold PBS (200*g*; 2 min; 4 °C) to remove traces of serum. Cells were pelleted in a final centrifugation step at 200*g* and 4 °C for 5 min. Hypotonic swelling of whole, intact cells was induced by resuspending the cell pellet in five packed cell volume extraction buffer containing 20 mM Tris–HCl, pH 7.6, 50 mM 2-mercaptoethanol, 0.1 mM EDTA, 2 mM MgCl2, 1 mM phenylmethylsulfonyl fluoride supplemented with protease inhibitors (2 μg/ml aprotinin, 2 μg/ml leupeptin, 0.3 μg/ml benzamidinchlorid, 10 μg/ml trypsininhibitor) and incubation for 2 min at room temperature and for another 10 min on ice. Cells were finally lysed by adding NP-40 at a final concentration of 1 % (v/v) and lysates were homogenized by passing through a 20-gauge needle or equivalent through a 200 μl tip for three times. Nuclei were pelleted by centrifugation at 500*g* for 5 min at 4 °C and washed two to three times in extraction buffer containing 1 % NP-40. During the final washing step, a small portion of nuclei was microscopically examined for purity and integrity. Pure, intact nuclei were pelleted in a final centrifugation step at 500*g* and 4 °C for 5 min.

Sample preparation for flow cytometry

Pellets of whole cells (harvested via gentle trypsinization and washed as described above) and isolated nuclei were gently resuspended in cold PBS to yield a final concentration of 0.5×10^6 cells/nuclei per ml. Cells/nuclei were fixed by directly adding 16 % formaldehyde (methanol-free, aqueous solution, EM grade) to obtain a final concentration of 1.5 % formaldehyde. After 10-min room temperature incubation under constant, mild agitation on a rotator, samples were pelleted by centrifugation (500*g*; 5 min; 4 °C). The supernatant was roughly discarded by inverting the tube and cells/nuclei were resuspended in residual PBS/paraformaldehyde by pipetting. They were then permeabilized by slowly adding ice-cold 100 % methanol, while gently vortexing, to a final concentration of $\sim 0.5 \times 10^6$ cells/nuclei per ml and incubation on ice for 30 min.

For the simultaneous staining of protein and DNA, fixed and permeabilized samples were aliquoted into assay tubes (2×10^5 cells/nuclei in 400 μl methanol per tube), washed in 1 ml staining medium (PBS containing 0.5 % BSA), pelleted by centrifugation (500*g*; 3 min) and then resuspended and incubated in 100 μl staining medium for 10 min at room temperature (blocking step). An optimal amount of primary antibody (typically about 10 ng per 2×10^5 cells) was then added and incubated for 60 min at room temperature. After a single washing step in PBS/0.5 % BSA, cells/nuclei were resuspended in 100 μl staining medium and the fluorophore-labeled secondary antibody was added at a dilution of 1:500 and incubated for 30 min at room temperature. Samples were then washed with 1 ml PBS/0.5 % BSA and DNA was stained by adding 300 μl propidium iodide/RNase solution (0.25 mg/ml propidium iodide, 0.05 mg/ml RNase and 0.1 % Triton X-100 in citrate buffer, pH 7.8) or alternatively 300 μl DRAQ7 (3 μM in PBS). After incubation for 20 min at room temperature, samples were analyzed on the flow cytometer.

Data acquisition and analysis on the flow cytometer

Stained cells/nuclei were acquired with BD CellQuest Pro software at medium flow rate on a FACSCalibur cytometer equipped with 488 and 635-nm lasers, and emission filters for FITC (FL1), PE (FL2), Cy5-PE (FL3), and APC (FL4) (BD Biosciences). DNA data were collected in pulse height, area and width parameters and protein data in height parameters only. A total of 1.5×10^4–5×10^4 cells/nuclei per sample were collected in linear (FSC-H/forward scatter, FL2-A/propidium iodide or FL3-A/DRAQ7) and logarithmic (SSC/side scatter, FL1-H/Alexa 488) amplification mode.

Preliminary data analysis as an initial quality control of acquired data was performed with BD CellQuest Pro software. For extended data analysis, files in Flow Cytometry Standard format (with a.fcs file extension) were imported to FlowJo data analysis software. Doublet discrimination via DNA staining was performed on FL2/3-W versus FL2/3-A plots for whole cells and isolated nuclei with the latter being more prone to aggregation.

To study protein expression during continuous cell cycle progression, a two step-gating procedure was applied: Initial gating for G1, S and G2/M subsets was accomplished on two-dimensional plots of DNA (FL2/3-A) versus protein (FL1-H). Using a software-based, rectangular gating tool, G1 and G2/M subsets were further dissected according to cell size via FSC, while the S phase subset was directly dissected according to DNA content. So obtained cell

cycle subsets, reflecting ongoing cell cycle progression from early G1 to late G2 and M, were then plotted against the corresponding median fluorescence intensities (MFI, in arbitrary units) of the particular protein staining. Background correction was performed by subtracting signals obtained with the isotype control from those obtained with the specific antibody. Finally, this procedure was applied to whole cells and isolated nuclei. Data on cytoplasmic regulations were obtained by subtracting nuclear staining results from whole cell staining results. P/T (Peak-to-Through) ratios to evaluate the overall extent of fluctuation during the cell cycle were calculated by dividing the highest MFI by the lowest.

Results and discussion

Immortalized MEFs deficient for *TSC1* or *TSC2* (tuberous sclerosis gene 1 or 2), two potent negative regulators of mTORC1, are well-established models for mTOR hyperactivation (Zhang et al. 2003; Rosner and Hengstschläger 2011). Whole cell analyses of these cells are traditionally confined to immunoblotting, demonstrating increased S6 phosphorylation at S240/4, with amounts of total S6 remaining unaffected (Fig. 1a, left panel). Using flow cytometry, we could recapitulate these results, confirming basic suitability of the method for our approach (Fig. 1a, right panel).

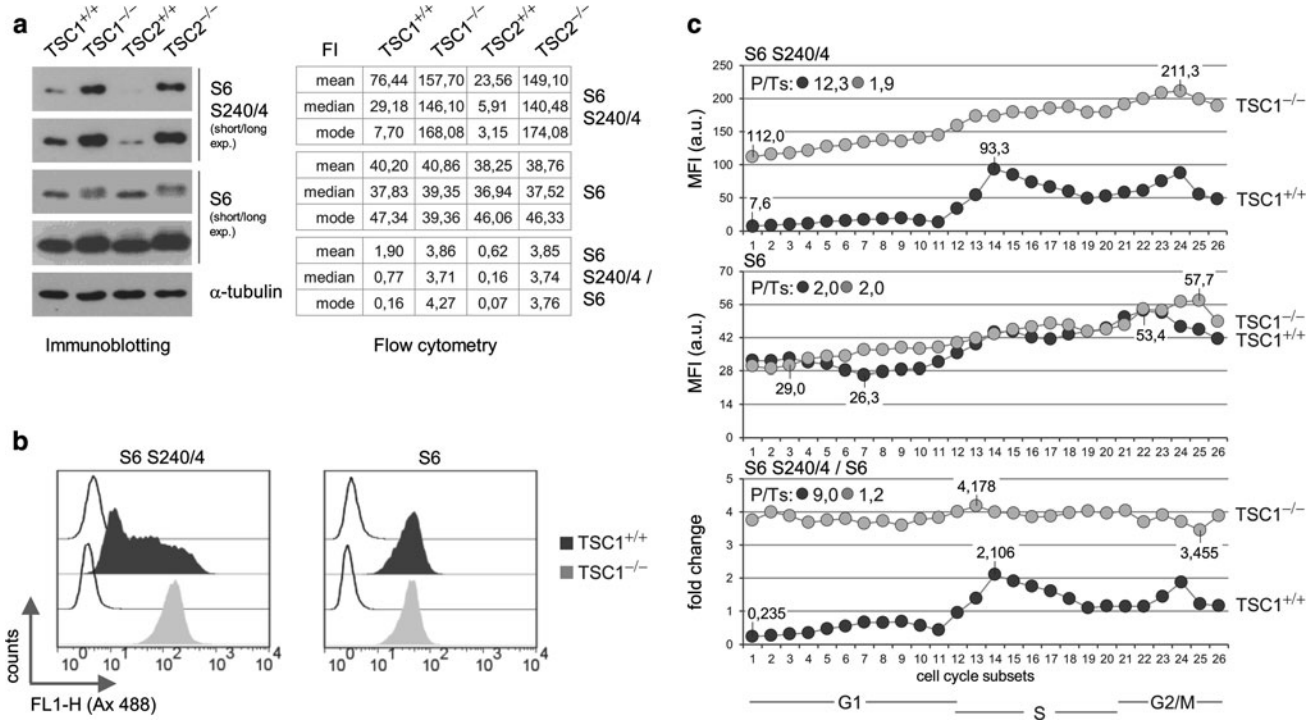

Fig. 1 Loss of TSC1 abrogates cell cycle-dependent expression of phosphorylated S6. **a** Immortalized *TSC1* and *TSC2* knockout MEFs and their wildtype counterparts were grown under full serum conditions for 72 h and harvested by mild trypsinization. Whole cells were either lysed or fixed, and subsequently analyzed for S240/4 phosphorylated and total forms of S6 via immunoblotting (*left panel*) and flow cytometry (*right panel*; the table summarizes mean, median and mode fluorescence intensity values obtained after whole cell staining with indicated antibodies). Results additionally include an α-tubulin reprobing as loading control (immunoblotting) and a data set on phosphorylated S6 after normalization to total S6 (S6 S240/4/S6) (flow cytometry). *FI* fluorescence intensity, *FI mode* fluorescence intensity value which is most frequently found for the given parameter. **b** Flow cytometric stagger histograms of S6 S240/4- and S6-stained *TSC1* wildtype and knockout cells analyzed in a (*open curves* control IgGs, *filled curves* specific IgGs). *FL1-H (Ax 488)* Alexa 488 (labeled antibody)-derived fluorescence (for details on the fluorescence staining procedure see "Materials and methods"). **c** Flow data shown in **b** were further analyzed involving a two step-gating procedure: data sets of cells dually labeled for protein (S6 S240/4 or S6) and DNA, were first gated for G1, S and G2/M subsets. G1 and G2/M subsets were further dissected according to cell size via FSC (*forward scatter*), the S phase subset was dissected according to DNA content. This finally allowed to establish a high-resolution map of protein expression during continuous cell cycle progression. Shown is the graph depiction of aligned cell cycle subsets (FSC subsets$_{(G1)}$/DNA subsets$_{(S)}$/FSC subsets$_{(G2/M)}$) (*X*-axis, 1–26), plotted against corresponding median fluorescence intensities (*MFI*) of the protein staining in arbitrary units (*a.u.*) (*Y*-axis). Results are shown for *TSC1* wildtype and knockout cells, labeled for phosphorylated and total S6 (*upper panels*; S6 S240/4 and S6) and phosphorylated S6 normalized to total S6 (*lower panel*; S6 S240/4/S6). Lowest and highest MFIs within each curve/cell population are numerically indicated. Thereof calculated P/T (Peak-to-Trough) ratios (MFI_{MAX}/MFI_{min}) are included in the *top left corner* of each graph (for details on the procedure see "Materials and methods")

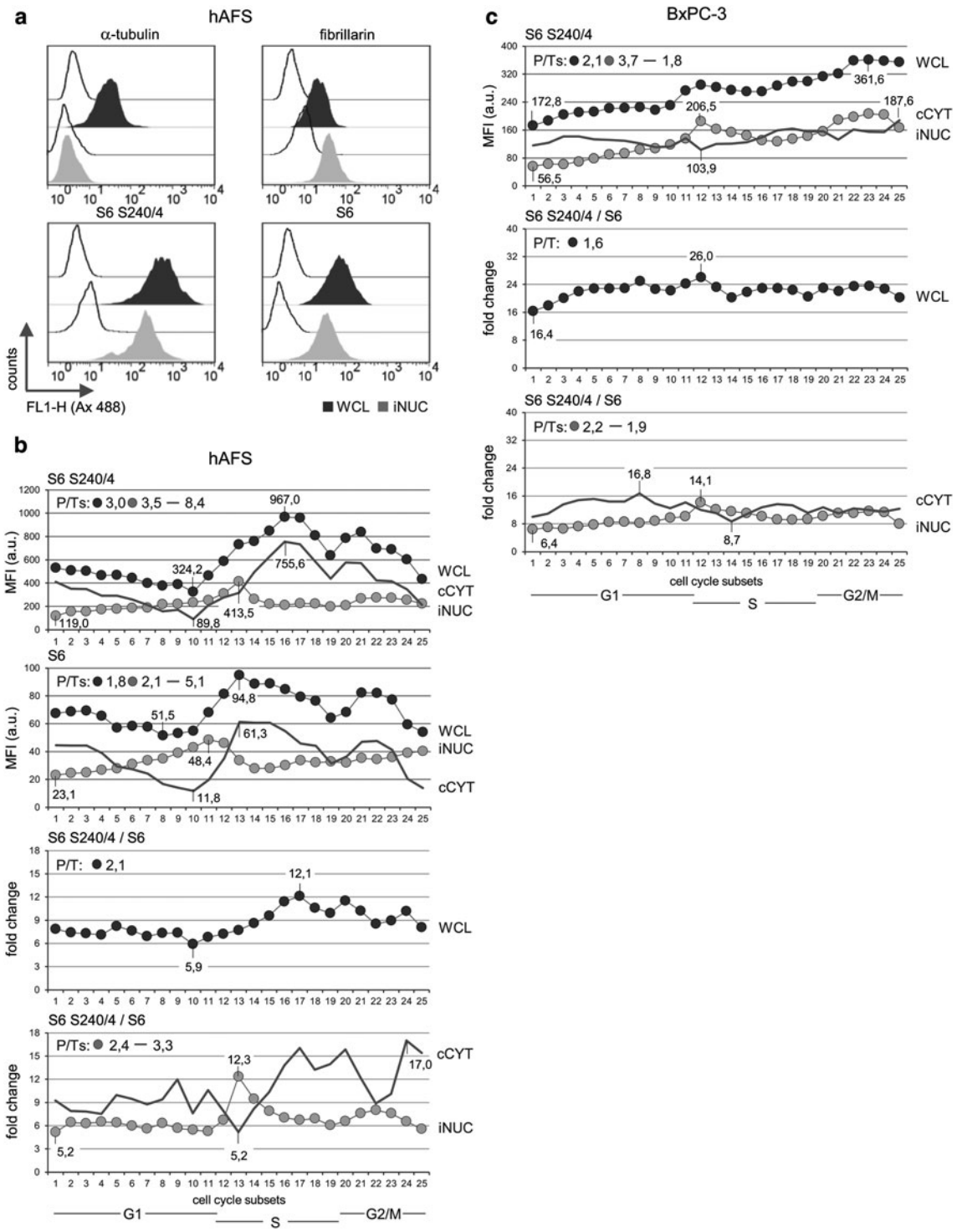

Since the tumor-suppressor protein p53 is known to be involved in S6-dependent pathways (Fumagalli et al. 2009), we focused on *TSC1* MEFs which, in contrast to *TSC2* MEFs, harbor a functional p53 gene (Zhang et al. 2003). Through the specific combination of flow cytometric DNA and cell size analyses, we established a high-resolution map of continuous cell cycle progression, reflecting early G1 to late G2 and M, to which S6 protein expression (Fig. 1b) was correlated (for details see the Figure legends and "Materials and methods"). As shown in Fig. 1c (top panel), we identified S240/4 phosphorylated S6 in *TSC1* wildtype MEFs as being strongly cell cycle-regulated, with lowest levels observed in G1, followed by a strong increase and a moderate decline in S, and a less pronounced, second peak in

◀ **Fig. 2** Phosphorylation of cytoplasmic and nuclear pools of ribosomal protein S6 during continuous cell cycle progression. **a** Flow cytometric stagger histograms of Q1 human amniotic fluid stem (*hAFS*) cells (*WCL*, whole cells) and isolated nuclei (*iNUC*) stained for α-tubulin, fibrillarin and phosphorylated and total S6 (*open curves* control IgGs, *filled curves* specific IgGs). **b** Cell cycle graphs were prepared as described for data in Fig. 1c and show the cell cycle regulation of phosphorylated (S6 S240/4) and total S6 (S6) in Q1 whole cells (*WCL*), isolated nuclei (*iNUC*) and thereof calculated cytoplasm (*cCYT*). Data on cytoplasmic regulations were obtained by subtracting nuclear staining results from whole cell staining results (*upper two panels*). In addition, graphs for phosphorylated S6 normalized to total S6 (S6 S240/4/S6) are presented for WCL and iNUC/cCYT (*lower two panels*). **c** Cell cycle graph of total and nucleocytoplasmic expression of phosphorylated S6 (S6 S240/4) in BxPC-3 pancreatic carcinoma cells (*upper panel*). Graphs for phosphorylated S6 normalized to total S6 (S6 S240/4/S6) are additionally presented for WCL and iNUC/cCYT (*lower two panels*). Lowest and highest MFIs within each curve/cell population are numerically indicated, and thereof calculated P/T (Peak-to-Trough) ratios (MFI_{MAX}/MFI_{min}) are included in the *top left corner* of each graph in **b** and **c**

G2/M. This finding differs from previous studies analyzing murine and human fibroblasts, which showed strong increase in S6 phosphorylation during exit from G0 into G1 and its steady decline during further cell cycle progression without any additional fluctuations being observed (Martin-Pérez and Thomas 1983; Rosner and Hengstschläger 2010). We believe this discrepancy to be due to the type of assay chosen: whereas mentioned previous approaches involve prior cell synchronization through serum depletion, the here used protocol allows to study protein expression during unperturbed cell cycle progression using asynchronously growing, unmanipulated cells. Prevailing, cell synchrony inducing procedures to enrich cells at a particular stage of the cell cycle are known to be associated with mild to severe perturbations of the cellular steady state (Darzynkiewicz et al. 2011). The classic block/release strategy of serum starvation/restimulation preferentially identifies serum-sensitive events upon re-entry of quiescent cells into the cell cycle, whereas events during unperturbed G1 progression or at later stages of the cell cycle, when synchrony rapidly declines, may not be fully detected. This might be of particular relevance when analyzing proteins involved in translation such as S6. Deviation between synchronization-dependent and -independent approaches is thus very likely to occur and was previously reported, e.g., for the cell cycle regulation of particular cyclins and cyclin-dependent kinase inhibitors (Darzynkiewicz et al. 2003).

Notably, loss of *TSC1* did not only cause a remarkable increase in S240/4 phosphorylated S6, (Fig. 1a, b) but completely abolished its cell cycle-dependent expression (Fig. 1c; top panel, compare P/T ratios of 12.3 and 1.9 for wildtype and knockout MEFs, respectively). When normalized to slightly fluctuating total S6 (Fig. 1c; middle panel), the effects of *TSC1* deletion became even more apparent (Fig. 1c; bottom panel; compare P/T 9.0 vs 1.2), providing evidence for constitutively elevated phosphorylation of S6 under conditions of hyperactivated mTOR.

To get a complete picture of S6 regulation under more physiological conditions, we co-evaluated cytoplasmic and nuclear compartments using hAFS cells. Therefore, we isolated nuclei, which we cytofluorometrically co-analyzed with whole cells. The used hypotonic/detergent fractionation protocol was already earlier proven to yield nuclei of high purity and integrity (Rosner and Hengstschläger 2011) and was shown to give similar results when compared to a sucrose-dependent approach (Hauser et al. 2002; unpublished data). Analyses of a defined panel of subcellular marker proteins via immunoblotting and flow cytometry confirmed the efficient nuclear recovery of soluble, low molecular weight proteins (such as S6), which are especially prone to purification-dependent leakage into the cytoplasm, e.g. c-jun, 43 kD; fibrillarin, 37 kD; and CENP-A, 17 kD (Rosner et al. 2011; Rosner and Hengstschläger 2011, 2012; and unpublished data). Moreover, we have shown that this protocol is suitable to perform fractionation of cells in different stages of the cell cycle, demonstrated by the recovery of comparable amounts of constitutively expressed, nuclear topoisomeraseIIβ in nuclear fractions of G0/G1-synchronized and released fractions (Rosner and Hengstschläger 2011).

In the here presented experiment, nuclear purity and integrity were proven by cytofluorometrically analyzing cytoplasmic (α-tubulin) and nucleolar (fibrillarin) marker proteins in whole cells versus isolated nuclei. Obtained results confirmed the absence of both, cytoplasmic contamination and leakage of isolated nuclei (compare the similar staining of fibrillarin in whole cells and isolated nuclei) (Fig. 2a, upper panels). In accordance with the literature, phosphorylated and total forms of S6 were mapped to both, whole cells and nuclei (Fig. 2a, lower panels) (Pende et al. 2004; Krüger et al. 2007; Rosner et al. 2011, 2012a). As shown for MEFs, we found hAFS cells to exhibit cell cycle-dependent regulation of S6 phosphorylated at S240/4, showing low G1 amounts and a similar "two-peak" pattern in S and G2/M (Fig. 2b, first graph, WCL). Fluctuation of total S6 during cell cycle progression, although less pronounced, was observed in wildtype MEFs and hAFS cells (Figs. 1c, middle panel, 2b, second graph, WCL). Support for the finding of non-constitutive, fluctuating S6 levels comes from a previous study on the synthesis and intracellular dynamics of ribosomal proteins including S6. It is argued that ribosomal proteins are expressed at much higher levels than actually needed for ribosome biogenesis what is balanced by the continuous proteosomal degradation of unassembled proteins in the nucleus (Lam et al. 2007). Importantly, cell cycle-dependent expression of phosphorylated S6 in hAFS cells

persisted even when normalized to total S6, albeit at lesser extent than in wildtype MEFs (Fig. 2b, third graph, WCL). However, low phosphorylation of S6 in G1, its increase in S and elevated expression in G2/M was observed for both, wildtype MEFs and hAFS cells.

Evaluation of co-analyzed nuclear and calculated cytoplasmic data sets revealed that the increasing expression of nuclear, S240/4 phosphorylated S6 during G1 is accompanied by an increase in the expression of nuclear, total S6. Nuclear, phosphorylated S6 reaches a maximum in early S, when levels of nuclear, total S6 begin to rapidly decline (Fig. 2b, first and second graph, iNUC). Concomitant to decreasing levels of nuclear, total S6 in early S, expression of cytoplasmic S6 (total and phosphorylated form) is strongly upregulated and peaks in mid (total S6) to late (phosphorylated S6) S (Fig. 2b, first and second graph, cCYT). Normalization of cytoplasmic and nuclear pools of phosphorylated S6 to total S6 confirmed the sharp increase in nuclear S6 phosphorylation in early S and the upregulation of cytoplasmic S6 phosphorylation in mid and late S (Fig. 2b, bottom graph, iNUC and cCYT).

Finally, we demonstrate that, comparable to *TSC1* knockout MEFs, human BxPC-3 pancreatic carcinoma cells show only minor fluctuation of S240/4 phosphorylated S6 (Fig. 2c; upper panel, WCL). Normalization of phosphorylated to total S6 showed that the specific pattern of increased phosphorylation in S and G2/M observed for wildtype MEFs and hAFS cells could not be detected (Fig. 2c; middle panel, WCL). Indeed, S6 phosphorylation in BxPC-3 appeared similarly constitutive as in knockout MEFs (Fig. 1c; bottom panel). Investigation of nucleocytoplasmic levels of phosphorylated S6 after normalization to total S6 revealed a pattern of slightly increased phosphorylation of nuclear S6 in early S (similar to hAFS cells), but no specific fluctuations in the phosphorylation of cytoplasmic S6 (Fig. 2c; bottom panel, iNUC and cCYT). The lack of the otherwise increased phosphorylation of cytoplasmic S6 in S (wildtype MEFs and hAFS cells) could be assumed to be the reason for the more constitutive S6 phosphorylation in BxPC-3 whole cells. These cells are known to exert hyperactivation of mTOR, what is suggested to be in part due to the constitutive activation of the mTOR regulating kinase Akt, triggered by promoter hypermethylation and diminished expression of the tumor suppressor PTEN (Asano et al. 2004; Chang et al. 2009; Glienke et al. 2012). We assume that the identified pattern of constitutive S6 phosphorylation during cell cycle progression in BxPC-3 cells might be a direct or indirect consequence of deregulated mTOR activity, as suggested for *TSC1*-deficient MEFs.

Collectively, we provide first evidence for the fluctuation of nucleocytoplasmic S6 phosphorylation during ongoing, unperturbed cell cycle progression and its aberrant regulation under conditions of deregulated mTOR activity. This finding has the potential to increase our knowledge about basic S6 regulation and may help to conclude on the compartment- and cell cycle stage-specificity of known S6 regulators and targets. On the other hand, these results may contribute to the in-depth understanding of the molecular consequences of mTOR deregulation. We have previously shown that mTOR-dependent phosphorylation of the S6 kinase p70S6K1 triggers its cell cycle-dependent nuclear localization (Rosner and Hengstschläger 2011). It is tempting to speculate that aberrant nuclear expression of functional p70S6K1 causes activation or inactivation of known and not yet identified nuclear targets (including S6), leading to their subcellular redistribution and/or aberrant activation during cell cycle progression. However, the functional link between nuclear p70S6K1 and nuclear S6, if any, remains to be established. Overall, the combination of cell cycle and localization studies as described here may help to establish spatiotemporal patterns of whole signaling cascades what could finally impact the targeted design of anti-tumor therapies by exploiting the spatiotemporal consequences of target inhibition (Rosner et al. 2012b).

Acknowledgments The clonal human amniotic fluid stem (hAFS) cell line Q1 was kindly provided by A. Atala (Wake Forest School of Medicine, Winston Salem, USA). Immortalized p53-positive *TSC1* (hamartin) and p53-negative *TSC2* (tuberin) wildtype and knockout cells were obtained from Dr. D. J. Kwiatkowski (Brigham and Women's Hospital, Boston, USA).

Conflict of interest The authors declare that they have no conflict of interest.

References

Asano T, Yao Y, Zhu J, Li D, Abbruzzese JL, Reddy SA (2004) The PI3-kinase/Akt signaling pathway is activated due to aberrant Pten expression and targets transcription factors NF-kappaB and c-Myc in pancreatic cancer cells. Oncogene 23:8571–8580

Bendall SC, Nolan GP (2012) From single cells to deep phenotypes in cancer. Nat Biotechnol 30:639–647

Chang Q, Chen E, Hedley DW (2009) Effects of combined inhibition of MEK and mTOR on downstream signaling and tumor growth in pancreatic cancer xenograft models. Cancer Biol Ther 8:1893–1901

Cisterna B, Biggiogera M (2010) Ribosome biogenesis: from structure to dynamics. Int Rev Cell Mol Biol 284:67–111

Darzynkiewicz Z, Juan G, Traganos F (2003) Cytometry of cell cycle regulatory proteins. Prog Cell Cycle Res 5:533–542

Darzynkiewicz Z, Halicka HD, Zhao H, Podhorecka M (2011) Cell synchronization by inhibitors of DNA replication induces replication stress and DNA damage response: analysis by flow cytometry. Methods Mol Biol 761:85–96

Fumagalli S, Di Cara A, Neb-Gulati A, Natt F, Schwemberger S, Hall J, Babcock GF, Bernardi R, Pandolfi PP, Thomas G (2009) Absence of nucleolar disruption after impairment of 40S ribosome biogenesis reveals an rpL11-translation-dependent mechanism of p53 induction. Nat Cell Biol 11:501–508

Glienke W, Maute L, Wicht J, Bergmann L (2012) The dual PI3 K/mTOR inhibitor NVP-BGT226 induces cell cycle arrest and regulates Survivin gene expression in human pancreatic cancer cell lines. Tumour Biol 33:757–765

Hauser C, Schuettengruber B, Bartl S, Lagger G, Seiser C (2002) Activation of the mouse histone deacetylase 1 gene by cooperative histone phosphorylation and acetylation. Mol Cell Biol 22:7820–7830

Krüger T, Zentgraf H, Scheer U (2007) Intranucleolar sites of ribosome biogenesis defined by the localization of early binding ribosomal proteins. J Cell Biol 177:573–578

Kundu-Michalik S, Bisotti MA, Lipsius E, Bauche A, Kruppa A, Klokow T, Kammler G, Kruppa J (2008) Nucleolar binding sequences of the ribosomal protein S6e family reside in evolutionary highly conserved peptide clusters. Mol Biol Evol 25:580–590

Lam YW, Lamond AI, Mann M, Andersen JS (2007) Analysis of nucleolar protein dynamics reveals the nuclear degradation of ribosomal proteins. Curr Biol 17:749–760

Laplante M, Sabatini DM (2012) mTOR signaling in growth control and disease. Cell 149:274–293

Ma XM, Blenis J (2009) Molecular mechanisms of mTOR-mediated translational control. Nat Rev Mol Cell Biol 10:307–318

Martin-Pérez J, Thomas G (1983) Ordered phosphorylation of 40S ribosomal protein S6 after serum stimulation of quiescent 3T3 cells. Proc Natl Acad Sci USA 80:926–930

Meyuhas O (2008) Physiological roles of ribosomal protein S6: one of its kind. Int Rev Cell Mol Biol 268:1–37

Pende M, Um SH, Mieulet V, Sticker M, Goss VL, Mestan J, Mueller M, Fumagalli S, Kozma SC, Thomas G (2004) S6K1(−/−)/S6K2(−/−) mice exhibit perinatal lethality and rapamycin-sensitive 5′-terminal oligopyrimidine mRNA translation and reveal a mitogen-activated protein kinase-dependent S6 kinase pathway. Mol Cell Biol 24:3112–3124

Perl AE, Kasner MT, Shank D, Luger SM, Carroll M (2012) Single-cell pharmacodynamic monitoring of S6 ribosomal protein phosphorylation in AML blasts during a clinical trial combining the mTOR inhibitor sirolimus and intensive chemotherapy. Clin Cancer Res 18:1716–1725

Rosner M, Hengstschläger M (2010) Evidence for cell cycle-dependent, rapamycin-resistant phosphorylation of ribosomal protein S6 at S240/244. Amino Acids 39:1487–1492

Rosner M, Hengstschläger M (2011) Nucleocytoplasmic localization of p70 S6K1, but not of its isoforms p85 and p31, is regulated by TSC2/mTOR. Oncogene 30:4509–4522

Rosner M, Hengstschläger M (2012) Detection of cytoplasmic and nuclear functions of mTOR by fractionation. Methods Mol Biol 821:105–124

Rosner M, Fuchs C, Dolznig H, Hengstschläger M (2011) Different cytoplasmic/nuclear distribution of S6 protein phosphorylated at S240/244 and S235/236. Amino Acids 40:595–600

Rosner M, Schipany K, Hengstschläger M (2012a) p70 S6K1 nuclear localization depends on its mTOR-mediated phosphorylation at T389, but not on its kinase activity towards S6. Amino Acids 42:2251–2256

Rosner M, Schipany K, Hengstschläger M (2012b) Spatial consequences of blocking mTOR/S6 K: relevance for therapy. Cell Cycle 11:420–421

Roux PP, Shahbazian D, Vu H, Holz MK, Cohen MS, Taunton J, Sonenberg N, Blenis J (2007) RAS/ERK signaling promotes site-specific ribosomal protein S6 phosphorylation via RSK and stimulates cap-dependent translation. J Biol Chem 282:14056–14064

Zhang Y, Lu H (2009) Signaling to p53: ribosomal proteins find their way. Cancer Cell 16:369–377

Zhang H, Cicchetti G, Onda H, Koon HB, Asrican K, Bajraszewski N, Vazquez F, Carpenter CL, Kwiatkowski DJ (2003) Loss of Tsc1/Tsc2 activates mTOR and disrupts PI3 K-Akt signaling through downregulation of PDGFR. J Clin Invest 112:1223–1233